plete energy randomization. The translational energy dependence of the $Cl^- + CH_3Br$ S_N2 reaction (*5*, *8*), for example, is significantly greater than that predicted by statistical theory (*16*) and differs dramatically from the observed temperature dependence of that reaction (*5*). Graul and Bowers (*14*, *15*) have shown that the kinetic energy release distribution (KERD) of the product ions of exothermic halide–methyl halide S_N2 reactions is significantly lower than that predicted by statistical models, and the product neutral is therefore internally "hot."

Both the translational energy and KERD experiments represent cases in which an ion-molecule complex is formed with energy partitioned nonstatistically between the vibrational and relative translational modes of the two species. Increased translational energy between reactants leads to a reactant complex formed with excited translational modes, whereas the neutral molecule in the product complex is vibrationally hot as a result of the reaction exothermicity. In both cases, poor translation-vibrational coupling in the S_N2 intermediate complex prevents statistical redistribution of energy.

The nonstatistical behavior of the halide–methyl halide systems may reflect the short lifetimes (10 to 100 ps) (*7*) of their intermediate complexes, which Boering and Brauman have shown to be a determining factor of the efficiency of intermolecular vibrational energy transfer (*18*). The short lifetimes are a result of the small size and low association energies (~10 kcal mol^{-1}) (*14*, *19*) of halide–methyl halide complexes, which are not typical of many ion-molecule reactions. The association energy of $[Cl{\cdot}ClCH_2CN]^-$, for example, is ~19 kcal mol^{-1} (*10*). Moreover, the internal vibrations of the neutral molecules have significantly different frequencies (for example, the methyl umbrella mode of CH_3Br differs from similar modes in $ClCH_2CN$) that might influence coupling. Although the limits of poor energy redistribution are yet to be determined, our results for Eq. 1 show that gross nonstatistical dynamics are not general to all gas-phase S_N2 reaction intermediates.

REFERENCES AND NOTES

1. K. A. Boering, J. Rolfe, J. I. Brauman, *Rapid Commun. Mass Spectrom.* **6**, 303 (1992); *Int. J. Mass Spectrom. Ion Processes* **117**, 357 (1992).
2. There is a slight off-resonance effect on the nonresonant ions (*3*), but it is negligible at these powers and frequencies.
3. J. W. Gauthier, T. R. Trautman, D. B. Jacobson, *Anal. Chim. Acta* **246**, 211 (1991).
4. G. Caldwell, T. F. Magnera, P. Kebarle, *J. Am. Chem. Soc.* **106**, 959 (1984); T. F. Magnera and P. Kebarle, in *Ionic Processes in the Gas Phase*, M. A. Almoster Ferreira, Ed. (Reidel, Dordrecht, Netherlands, 1984), vol. 118, pp. 135–157.
5. A. A. Viggiano, R. A. Morris, J. S. Paschkewitz, J. F. Paulson, *J. Am. Chem. Soc.* **114**, 10477 (1992).
6. A. A. Viggiano *et al.*, *ibid.* **116**, 2213 (1994).
7. C. Li, P. Ross, J. E. Szulejko, T. B. McMahon, *ibid.* **118**, 9360 (1996).
8. S. L. Craig and J. I. Brauman, *J. Phys. Chem.*, in press.
9. B. D. Wladkowski, K. F. Lim, W. D. Allen, J. I. Brauman, *J. Am. Chem. Soc.* **114**, 9136 (1992).
10. T. Su, *J. Chem. Phys.* **100**, 4703 (1994).
11. R. A. Marcus, *ibid.* **20**, 359 (1952); ———, W. L. Hase, K. N. Swamy, *J. Phys. Chem.* **88**, 6717 (1984); W. Forst, *Theory of Unimolecular Reactions* (Academic Press, New York, 1973); R. G. Gilbert and S. C. Smith, *Theory of Unimolecular and Recombination Reactions*, J. P. Simons, Ed. (Physical Chemistry Texts, Blackwell Scientific, Oxford, 1990); P. J. Robinson and K. A. Holbrook, *Unimolecular Reactions* (Interscience, London, 1972).
12. For a given translational energy, the center-of-mass collision energy in excess of the thermal value (0.045 eV at 350 K) is converted to an increased temperature of the reactants. Orbital angular momentum is conserved, and the increased fixed rotational energy is calculated from a classical collision model. The collision rate is calculated according to (*10*), and branching in the collision complex is then treated microcanonically (*9*) at the increased temperature.
13. W. L. Hase, *Science* **266**, 998 (1994); M. V. Basilevsky and V. M. Ryaboy, *Chem. Phys. Lett.* **129**, 71 (1986); V. M. Ryaboy, *ibid.* **159**, 371 (1989); S. R. Vande Linde and W. L. Hase, *J. Am. Chem. Soc.* **111**, 2349 (1989); *J. Phys. Chem.* **94**, 6148 (1990); *ibid.*, p. 2778; *J. Chem. Phys.* **93**, 7962 (1990); Y. J. Cho, S. R. Vande Linde, L. Zhu, W. L. Hase, *ibid.* **96**, 8275 (1992); H. Wang, G. H. Peslherbe, W. L. Hase, *J. Am. Chem. Soc.* **116**, 9644 (1994); G. H. Peslherbe, H. Wang, W. L. Hase, *J. Chem. Phys.* **102**, 5626 (1995); A. A. Viggiano and R. A. Morris, *J. Phys. Chem.* **100**, 19227 (1996); H. Wang and W. L. Hase, *Chem. Phys.* **212**, 247 (1996).
14. S. T. Graul and M. T. Bowers, *J. Am. Chem. Soc.* **113**, 9696 (1991).
15. ———, *ibid.* **116**, 3875 (1994).
16. H. Wang and W. L. Hase, *ibid.* **117**, 9347 (1995).
17. Earlier investigation of the translational energy dependence of Eq. 1 (*6*) did not cover a large enough energy range to be conclusive.
18. K. A. Boering and J. I. Brauman, *J. Chem. Phys.* **97**, 5439 (1992).
19. J. E. Bartmess, NIST Negative Ion Energetics Database, Version 3.0 (Standard Reference Database 19B, National Institute of Standards and Technology, Gaithersburg, MD, 1993).

20. Supported by NSF. S.L.C. was supported by an NSF predoctoral fellowship, an American Chemical Society Division of Organic Chemistry DuPont Merck Pharmaceutical Fellowship, and a John Stauffer Memorial Fellowship.

4 February 1997; accepted 3 April 1997

Accessible Solitons

Allan W. Snyder* and D. John Mitchell

Solitons are ubiquitous. Their description involves abstruse mathematics and is limited to a two-dimensional idealization. A nonlocal model is presented that provides a radical simplification and allows for an elegant description of soliton collisions, interactions, and deformations in two and three dimensions. The model reveals an intimate connection between solitons and the linear harmonic oscillator. It foreshadows a photonic switch in which a bright beam can steer a distant dim beam, and it predicts the existence of noncircularly symmetric solitons.

Solitary waves create their own channel as they travel in a uniform medium, remaining localized and preserving their shape (*1*). But, they can be dramatically altered by colliding with one another (*2*). Solitons are solitary waves that are unaltered by collisions (*1*). The conventional models of soliton propagation are complex; we provide a simple model.

Consider the example of monochromatic light beams in a homogeneous medium whose (squared) refractive index (*3*) is $n^2 = n_L^2 + \delta n^2$. Here, n_L is the constant linear part of the refractive index, whereas δn^2 is the nonlinear induced change caused by the beam. Typical of many materials (*4*–*7*), δn^2 is positive and obeys $\delta n^2 \ll n_L^2$. The conventional model assumes an idealized local response when, by definition, δn^2 at position x is proportional to the beam's intensity at x. This local (Kerr) model admits solitons in two dimensions only. The resulting Schrödinger equation does not have explicit closed-form solutions, except for special initial conditions. Furthermore, the inverse scattering technique that is required for solution is excessively mathematical (*1*). This complexity is not fundamental to solitons, but rather, is a consequence of the specific model.

Consider a model of nonlinearity whose response is highly nonlocal. Then, by definition, a light beam of characteristic radius ρ creates a circularly symmetrical refractive index change δn^2 whose characteristic spatial extent is much larger than ρ and whose axis is set by the beam center and its initial direction. Consequently, δn^2 depends on the integrated intensity of the beam, or power, P. The situation of high nonlocality is analogous to observing distant point sources through a badly blurred lens. When the point sources (light beams) are sufficiently close to the lens axis, the shape of the blur circle (nonlocal response) is indis-

Institute of Advanced Studies, Australian National University, Canberra 0200, Australia.

*To whom correspondence should be addressed. E-mail: a.snyder@anu.edu.au

tinguishable from that due to one point source alone. At the other extreme, a local response is analogous to having a delta-function blur circle. Various materials exhibit a highly nonlocal response, including photorefractive materials (*5–7*), liquid crystalline materials (*8*), and materials that exhibit laser-induced thermal nonlinearities (*9*). The underlying physical processes for such nonlocality is also known (*10*). Advances by Segev *et al.* (*5*, *6*) suggest that photorefractive materials are the most suitable for investigating large nonlocality (*11*).

We now transcribe the nonlocal model into an expression for δn^2. The key idea is that the spatial extent of each light beam, as well as the distance between them, is negligible compared to the characteristic nonlocal response length of δn^2. Under these conditions, the refractive index δn^2 "seen" by the beams is that confined near the axis of δn^2. Thus, we need only keep the first two terms of a Taylor series. This leads to $\delta n^2(r, P) = \delta n^2(0, P) - r^2\alpha^2(P)$, where $r = |\mathbf{x} - \bar{\mathbf{x}}|$ is the transverse distance from the beam center. Substituting this into the expression for the refractive index, $n^2 = n_L^2 + \delta n^2$, leads to our model for nonlinearity

$$n^2(r,P) = n_0^2 - r^2\alpha^2(P) \qquad (1)$$

Here, $n_0 = n(0,P)$ is the maximum refractive index. $\alpha(P)$ is a given material property. It is real and $\alpha(0) \equiv 0$. We define a nonlocal Kerr medium as the special case when $\alpha^2(P) = \gamma^2 P$, where γ is a material constant. For optical materials (*4–6*), $n_0 \cong n_L$.

The interpretation of Eq. 1 is that a beam of power P induces a circularly symmetric, parabolic refractive index waveguide, $n(r,P)$. The axis at position $\bar{\mathbf{x}}$ of the induced refractive index is specified by the initial direction of the beam center. For example, $\bar{\mathbf{x}}$ for a Gaussian shaped beam of power P is located at the maximum of the beam with $\alpha = \alpha(P)$ in Eq. 1, whereas $\bar{\mathbf{x}}$ for two identical parallel beams of total power $2P$ is midway between the two maxima with $\alpha = \alpha(2P)$. Thus, each beam behaves differently from one alone.

The electric field E of light obeys Maxwell's equations which, for homogeneous nonlinear materials, are formally equivalent (*12*) to the familiar Schrödinger equation, $2ikn_0(\partial\psi/\partial z) + \nabla_\perp^2\psi + k^2(n^2 - n_0^2)\psi = 0$, where $E = \psi e^{ikn_0 z}$, $k = 2\pi/\lambda$, with λ the wavelength of light in vacuum, z the longitudinal coordinate, and $\nabla_\perp^2 = (\partial^2/\partial x^2) + (\partial^2/\partial y^2)$. Taking n^2 from Eq. 1, our defining equation for solitons is

$$2ikn_0(\partial\psi/\partial z) + \nabla_\perp^2\psi - k^2\alpha^2(P)r^2\psi = 0 \qquad (2)$$

where $r = |\mathbf{x} - \bar{\mathbf{x}}|$ is the transverse distance from the beam center and $P = \int|\psi|^2\,dx\,dy$ is the beam power. The initial conditions of the beam center at $\bar{\mathbf{x}}$, defined as the first moment of the intensity profile $|\psi|^2$, set the axis of this circularly symmetric system. We choose $\bar{\mathbf{x}} = 0$. This is the famous equation for the linear harmonic oscillator (*13*). Although linear in ψ, it nonetheless describes the highly nonlinear phenomenon of solitons through the dependence of the coefficient α on beam power P, a conserved quantity.

Soliton propagation is thus reduced to one of the simplest and best studied equations of linear physics. We merely borrow from the literature of the linear harmonic oscillator or equivalently from the propagation of light in a parabolic refractive index medium (*14*, *15*). Because the physics of these two classical problems is so well understood, we first translate it into the context of solitons. This imparts intuition before presenting the mathematics. For example, consider how a Gaussian beam will propagate in a highly nonlocal homogeneous medium when its initial width is fixed, but when its initial intensity, and hence its power, is changed. At zero power, $n = n_0$ in Eq. 1, and the beam diffracts as it does in a linear homogeneous medium. For finite power, the beam induces the parabolic index medium of Eq. 1 with its axis at the beam center. It is well known (*14*) that the beam preserves its Gaussian shape but its characteristic width "breathes" sinusoidally as it travels in a straight path. If $\alpha(P)$ in Eq. 1 is monotonically increasing, a critical power $P = P_c$ exists when beam diffraction is balanced by beam-induced refraction. This is a soliton. For $P > P_c$, refraction initially overcomes diffraction and the beam initially contracts, whereas for $P < P_c$, the reverse happens and the beam initially expands (Fig. 1, left).

Simple expressions can be derived to describe Gaussian beam propagation in an arbitrary, highly nonlocal medium. To do this, we substitute a Gaussian (trial) function into Eq. 2 as shown in (*16*). This leads to a closed-form expression for the intensity $I = |\psi|^2$ of the Gaussian beam as a function of spatial propagation distance z, where

$$I(z) = I_m(z)e^{-x^2/\rho^2(z)} \qquad (3)$$

with $I_m(z) = P/\rho(z)\sqrt{\pi}$ for two-dimensional (2D) beams. For 3D beams, $I_m(z) = P/\pi\rho^2(z)$, with x in Eq. 3 replaced by the radial position r. The characteristic half-width or radius has the simple form

$$\frac{\rho^2(z)}{\rho_0^2} = \cos^2 qz + \frac{\alpha^2(P_c)}{\alpha^2(P)}\sin^2 qz \qquad (4)$$

where ρ_0 is the initial beam width, $q = \alpha(P)/n_0$, and the critical power P_c is defined by $\alpha(P_c) = 1/k\rho_0^2$. For the special case of a nonlocal Kerr medium, $\alpha^2(P) = \gamma^2 P$, where γ is a material constant. Then $P_c = 1/k^2\gamma^2\rho_0^4$ and $q = \gamma\sqrt{P}/n_0$.

Next, we discuss the interaction of two Gaussian beams. To impart intuition, we again translate the physics from the classical

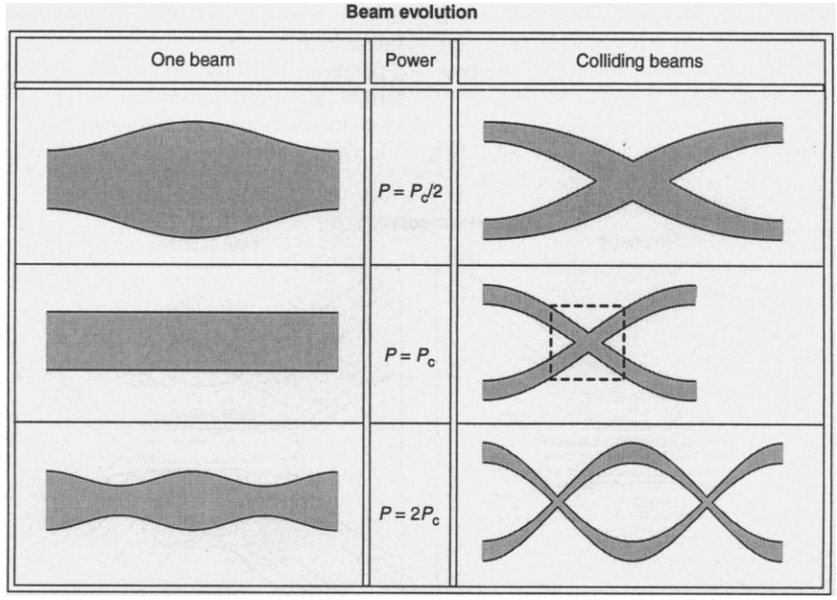

Fig. 1. Gaussian beam propagation in a highly nonlocal Kerr medium. The initial beam width is the same in all cases, but the intensity, and hence, the power P is changed. The characteristic beam width or diameter is stationary only when $P = P_c$, otherwise it changes sinusoidally as shown on the left for a single beam and on the right for two beams. Two identical beams, initially in parallel, will strongly interact and periodically collide as shown on the right. The interference within the boxed overlap zone is shown in Fig. 2 for coherent beams.

problem of propagation in a parabolic medium (*14, 15*) before we give the mathematics. When two identical Gaussian beams, of total power P, are launched in parallel, they "see" a different parabolic medium, one characterized by $\alpha = \alpha(P)$ in Eq. 1, rather than one beam alone of power $P/2$, for which $\alpha = \alpha(P/2)$. The axis of this medium is midway between the two maxima of the beams. For zero power, $\alpha = 0$ and the medium is homogeneous. Each beam then diffracts as it travels in a straight path. For finite power, each beam is parallel to but displaced from the axis of the induced parabolic medium. Such beams are well known to undergo sinusoidal trajectories about the axis of the parabolic medium. Accordingly, two initially parallel beams of a highly nonlocal nonlinearity will strongly interact and undergo periodic collisions, with the period depending on P, but each beam retains the same form as the isolated beam of power P discussed above (Fig. 1, right). The beam trajectories are dictated by paraxial ray optics (*17*). Beams are unaltered by collision. Phase plays no role other than interference (*18*) as shown in Fig. 2. In three dimensions, two beams will spiral about one another, like rays in a parabolic index medium (*15*), if they are initially skew to each other.

Simple closed-form expressions describe these interacting Gaussian beams. We find (*17*) that the trajectory $\boldsymbol{x}_0$ of each beam center obeys the paraxial ray equation, $(d^2\boldsymbol{x}_0/dz^2) = -(\alpha/n_0)^2\boldsymbol{x}_0$, so that $x_0(z) = x_0(0)\cos(qz)$ with $q = \alpha(P)/n_0$, when the beams are initially parallel. The summed beam intensity $I(x + x_0) + I(x - x_0)$ is shown on the right side of Fig. 1 and is given by Eq. 3 replacing x with $(x \pm x_0)$. The expression (*17*) for the composite two-beam intensity (Fig. 2) is

$$(I/A) = I_+ + I_- \pm 2\sqrt{I_+ I_-}\cos\theta \quad (5)$$

where $I_\pm$ is $I(x \pm x_0)$ in Eq. 3, and A is chosen so that the power is P. For solitons ($P = P_c$), then $\rho_0^2\theta = 2x_0(0)x\sin(qz)$, with $\rho(z) = \rho_0$, $k\rho_0^2\alpha(P_c) = 1$, and $2A = \{1 + e^{-x_0^2(0)/\rho_0^2}\}^{-1}$.

Finally, suppose the above two Gaussian beams have the same width but that one has power, $P_c - \delta$, whereas the other has power, δ, where $\delta \to 0$. It can then be shown (*19*) that the "bright" beam of power $P_c - \delta$ travels straight as if it were in isolation. The "dim" beam of power, δ, remains uniform but oscillates about the bright beam in a sinusoidal trajectory. It would diffract and travel in a straight path if it is in isolation. This finding has implications to photonic switching (*18, 20*) in that a "distant" dim beam can be steered by a soliton.

Our results for Gaussian beams follow by direct substitution in Eq. 2. An arbitrary beam also undulates sinusoidally. Its center also follows paraxial ray optics, but its shape changes (*17*). In general, an arbitrary field ψ of Eq. 2 can be represented by a linear sum of solitons $\psi_n e^{i\beta_n z}$. The Hermite-Gauss functions ψ_n form a complete set (*14, 15*). The Gaussian is the lowest order soliton. Unlike a local medium, noncircularly symmetric solitons exist in a highly nonlocal nonlinear medium. Because the eigenvalues β_n are equally spaced, all solutions of Eq. 2 are sinusoidal.

In summary, the traditional model for solitons requires abstruse mathematics and is limited to a 2D, cubic (Kerr) nonlinearity, whereas solitons of a highly nonlocal medium obey one of the simplest and best studied equations of linear physics. We merely borrow from the literature of the linear harmonic oscillator or propagation in a parabolic refractive index medium to obtain an elegant description of soliton collisons, interactions, and deformations in two and three dimensions for both cubic (Kerr) and non-Kerr nonlinearities. An arbitrary initial field can be formally expressed as a linear superposition of solitons.

It would appear that a highly nonlocal nonlinearity offers the simplest model possible for introducing the concept of a soliton (*21*).

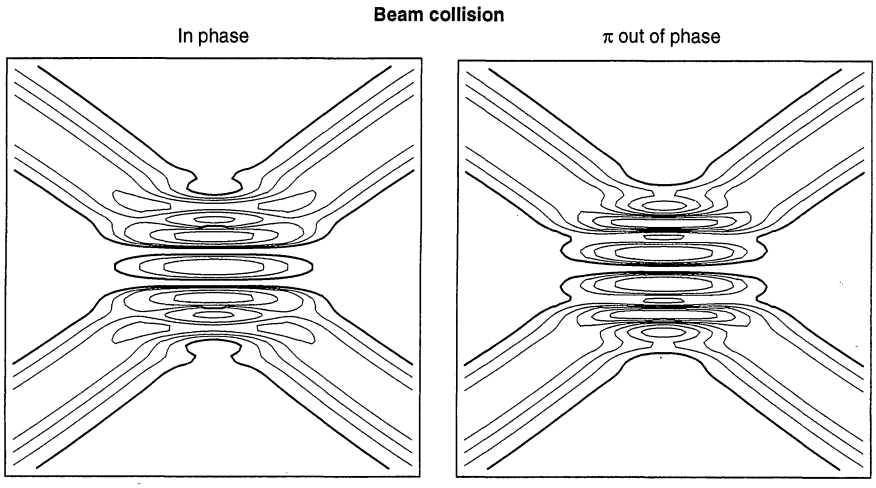

Fig. 2. The intensity contours for two colliding solitons in the region shown by the dashed square on the right side of Fig. 1. The beams are in phase on the left (constructive interference) and π out of phase on the right (destructive interference) as discussed in (*17*).

REFERENCES AND NOTES

1. P. G. Drazin and R. S. Johnson, *Solitons: An Introduction* (Cambridge Univ. Press, Cambridge, 1989); P. G. Drazin, *New Sci.* **132**, 28 (1991); V. E. Zakharov and A. B. Shabat, *Sov. Phys. JETP* **34**, 62 (1972).
2. A. W. Snyder and A. P. Sheppard, *Opt. Lett.* **18**, 499 (1993).
3. We follow the convention of modern optics by working with n^2, the quantity appearing in Maxwell's equations, rather than n.
4. Y. Silberberg, *Spatial Optical Solitons; Experiments and Advances in Integrated Optics*, S. Martilucci, A. N. Chester, M. Bertolotti, Eds. (Plenum, New York, 1994).
5. M. Segev, B. Crosignani, A. Yariv, B. Fischer, *Phys. Rev. Lett.* **68**, 923 (1992).
6. G. Duree *et al.*, *ibid.* **71**, 533 (1993).
7. P. Gunter, *Phys. Rep.* **93**, 199 (1982); P. Yeh, *Introduction to Photorefractive Nonlinear Optics* (Wiley, New York, 1993).
8. I. C. Khoo, *Prog. Opt.* **26**, 107 (1988).
9. J. P. Gordon, R. C. C. Leite, R. S. Moore, S. P. S. Porto, J. R. Whinnery, *J. Appl. Phys.* **36**, 3 (1965).
10. The physical mechanism for nonlocality in laser-induced thermal nonlinearities (*9*) is thermal diffusion. High nonlocality occurs when the characteristic diffusion length exceeds the characteristic width of the light beam. In photorefractive materials (*5–7*), the nonlocal response typically arises where it is induced by the photogeneration of carriers that diffuse far away from the illuminated region and are captured by traps. This leads to an extended electric field that modulates the refractive index through the electrooptic effect.
11. No systematic investigation of solitons is available in the highly nonlocal regime where the material response length exceeds the characteristic beam width. Meaningful comparisons with the predictions of our paper are thus premature. They are best facilitated in photorefractive materials with large Debye lengths. (M. Segev, personal communication)
12. Maxwell's equation for the transverse electric field E is equivalent [section 8 of (*22*)] to the Schrödinger equation, provided only that $n \cong n_0$ in Eq. 1. This is satisfied for realistic nonlinear materials.
13. L. I. Schiff, *Quantum Mechanics* (McGraw-Hill, New York, 1968).
14. J. Arnaud, *Beam and Fibre Optics* (Academic Press, New York, 1976), p. 52; *ibid.*, p. 64.
15. A. W. Snyder and J. D. Love, *Optical Waveguide Theory* (Chapman and Hall, London, 1983), p. 43; *ibid.*, p. 306.
16. The complex Gaussian $\psi = (b)^{1/2}\exp(ax^2)$ satisfies the 2D form of Eq. (2), where b and a are complex functions of axial distance z, provided $a = ikn_0\dot{b}/(2b)$ and $\ddot{b} + (\alpha^2/n_0^2)b = 0$, where $\dot{b} \equiv db/dz$. This is verified by direct substitution. The result in 3D is found by separation of variables, where $\psi = \psi(x, b_1)\psi(y, b_2)$. The half-width or radius ρ is given by $(1/\rho^2) = -2\mathrm{Re}(a)$, where Re signifies the real part. Algebra then leads to Eq. 4. The maximum intensity $I_m = |b|$.
17. It is well known (*14*) that the beam center $\boldsymbol{x}_0$ of a single beam travelling in a (linear) parabolic-index medium satisfies the paraxial ray equation, $d^2\boldsymbol{x}_0/dz^2 = -(\alpha/n_0)^2\boldsymbol{x}_0$. The beam shape is independent of its motion. An analogous result holds in quantum mechanics (*13*) for the linear harmonic oscillator, where the mean position of the oscillator satisfies Newton's equation. These results follow from the observation that, if $\psi(\boldsymbol{x}, z)$ is a solution of Eq. 2, so is $\psi(\boldsymbol{x} - \boldsymbol{x}_0, z)\exp(i\boldsymbol{u}\cdot\boldsymbol{x} + i\phi)$, where and $\boldsymbol{u} = kn_0\dot{\boldsymbol{x}}_0$, and $2kn_0\dot{\phi} = k^2(\alpha^2\boldsymbol{x}_0^2 - n_0^2\dot{\boldsymbol{x}}_0^2)$, provided $\boldsymbol{x}_0$ satisfies the ray equation. This is verified by substitution. To

obtain Eq. 5, we take the magnitude squared of the sum of the fields for two identical beams in phase or 180° out of phase, $\psi(x - x_0,z)\exp(iu \cdot x + i\phi) \pm \psi(x + x_0,z)\exp(-iu \cdot x + i\phi)$, multiplied by a normalizing constant to set the total power to P. The relative phase is $\theta = -2u \cdot x$, where $u = -kn_0\, qx(0)\sin(q,z)$.

18. For a given power, the trajectory is independent of phase, unlike in a local nonlinearity [L. Poladian, A. W. Snyder, D. J. Mitchell, *Opt. Commun.* **85**, 59 (1991)].
19. The parabolic medium induced by the two beams depends on their total power $P_c - \delta$ through the coefficient $\alpha(P)$ in Eq. 1, so $\alpha \cong \alpha(P_c)$. The axis of this parabolic medium is determined by the first moment of the composite two-beam intensity distribution as discussed below Eq. 2. It is thus centered approximately on the bright beam. Propagation then follows from the physics of the parabolic medium (*14, 15*). The dim beam is displaced from the axis and so undergoes sinusoidal oscillations about the bright beam, whereas the on-axis bright beam travels straight. Further, the dim and bright beam have the same width—that necessary to remain uniform in the $\alpha \cong \alpha(P_c)$ parabolic medium.
20. Y. Silberberg, *Opt. News* **15**, 7 (1989).
21. We previously (*22, 23*) showed that linear physics provides deep insight into the soliton dynamics of a local nonlinear medium, but large nonlocality allows us to demonstrate the concept with particular elegance and to obtain exact closed-form expressions for collisions.
22. A. W. Snyder, D. J. Mitchell, Y. S. Kivshar, *Mod. Phys. Lett. B* **9**, 1479 (1995).
23. A. W. Snyder, *Opt. Photonics News* **7**, 17 (1996); _____ and D. J. Mitchell, *Opt. Lett.* **22**, 16 (1997); A. W. Snyder, S. J. Hewlett, D. J. Mitchell, *Phys. Rev. Lett.* **72**, 1012 (1994).

24. We thank N. Akhmediev, P. Chiao, Y. Kivshar, F. Ladouceur, M. Segev, and R. Shen for insight. The authors are part of the Australian Photonics Cooperative Research Centre.

13 January 1997; accepted 14 April 1997

Preservation of Chitin in 25-Million-Year-Old Fossils

B. Artur Stankiewicz, Derek E. G. Briggs, Richard P. Evershed, Matthew B. Flannery, Michael Wuttke

Chitin is present in fossil insects from the Oligocene (24.7 million years ago) lacustrine shales of Enspel, Germany. This result, which was obtained by analytical pyrolysis, extends by nearly 25 million years the length of time that chemically detectable remains of this biomolecule are known to survive. The embedding sediment is dominated by diatoms, which reflect high productivity in the paleolake. The primary control on the preservation of chitin is thus not time; it may persist in older sediments where suitable paleoenvironmental conditions prevailed.

Chitin, which is one of the most abundant macromolecules on Earth, is also one of the most enigmatic of molecular fossils. An estimated 10^{11} tons of chitin is produced annually in the biosphere, most of it in the oceans (*1*). It occurs in a range of organisms but is particularly important as a constituent of arthropod cuticles (*1–4*), where it is cross-linked with proteins via catechol and histidyl moieties (*5*). Although biodegradation in the water column and sediment normally removes almost all of the chitin produced in the oceans (*3*), experiments have demonstrated that chitin is the component of shrimps that is most resistant to degradation (*6*) and organic remains of arthropod cuticle are abundant in the fossil record, in some cases preserving remarkable morphological detail (*7*). Chitin has been detected in insects in terrestrial deposits of Pleistocene age (~130,000 years ago) (*8*) and in asphalt deposits from California (*9*). However, analyses have failed to provide evidence for its presence in older fossils except (*6, 10–12*) for traces of amino sugars in the calcified skeletons of one Cretaceous and three Tertiary decapod crustaceans (*13*). Even where the morphology of the cuticle appears well preserved, the original chemical composition may be completely altered.

Pyrolysis–gas chromatography–mass spectrometry (py-GC-MS) (*6, 14–16*) provides a powerful tool for the chemical characterization of invertebrate cuticles (*9, 15*), particularly in cases in which the sample size is limited to a few micrograms. Investigation of the cuticles of fossil arthropods from 15 sites ranging in age from Silurian to Cretaceous revealed no trace of the original chemical components of chitin (*12*). The chemical signature either (i) was dominated by the *n*-alk-1-ene and *n*-alkane doublets characteristic of highly aliphatic biopolymers or (ii) contained a substantial aromatic component including alkylbenzenes and alkylindenes and relatively abundant sulfur-containing compounds such as thiophenes (*12*).

Here we demonstrate that chitin is preserved in the late Oligocene [24.7 million years ago (Ma)] Enspel Fossillagerstätte (*17*) near Bad Marienberg, in the Westerwald, Rheinland-Pfalz, Germany, where maar-lake deposits are interbedded with tuff

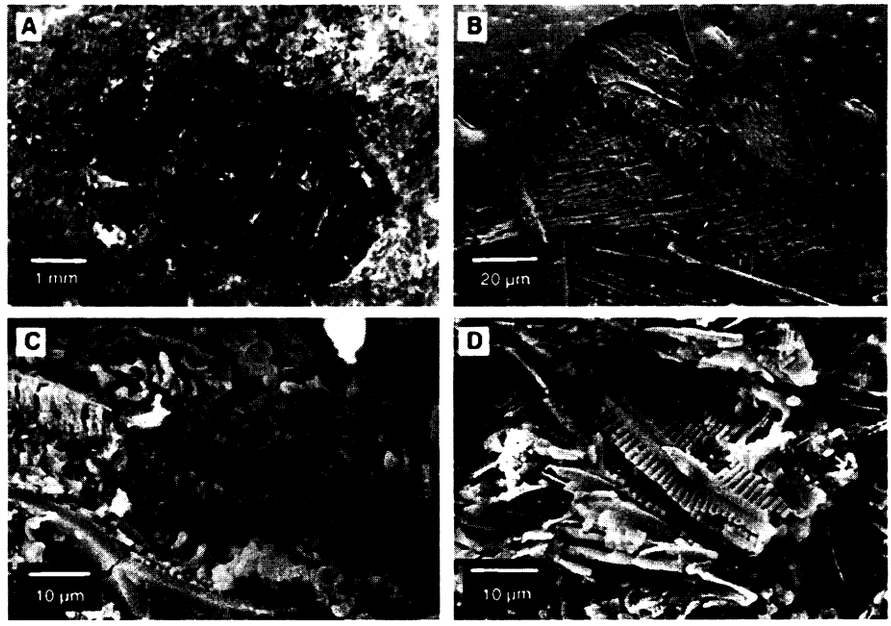

Fig. 1. Photomicrographs of (**A**) the ventral view of a beetle (Coleoptera: Curculionoidea) from level 12 of the Oligocene (24.7 Ma) of Enspel, western Germany; (**B**) an SEM image of the cuticle of a modern mealworm beetle (*Tenebrio molitor*) that reveals the layers of cuticle overlapping at different angles; (**C** an SEM image of a fractured edge of cuticle of the specimen illustrated in (A) that shows chitinous fibers; and **D**) an SEM image of the shale matrix that contains the fossil insects and reveals that pennate diatoms are the dominant constituent. (Images were made with a Cambridge Stereoscan 250 Mk3 SEM at 7 to 12 kV after specimens were coated with gold.)

B. A. Stankiewicz and D. E. G. Briggs, Biogeochemistry Research Centre, Department of Geology, University of Bristol, Queen's Road, Bristol BS8 1RJ, UK.
R. P. Evershed and M. B. Flannery, Organic Geochemistry Unit, School of Chemistry, University of Bristol, Cantock's Close, Bristol BS8 1TS, UK.
M. Wuttke, Landesamt für Denkmalpflege Rheinland-Pfalz, Referat Erdgeschichtliche Denkmalpflege, Am Obstmarkt 13, D-55126 Mainz, Germany.